Analysis of Electromagnetic Field of Radial Magnetic Levitation Bearings Based on Finite Element Simulation

Qinglai Wei, Moxuan Ren, Long Wang, Liang Li, and Yanbin Du

***Abstract*—A systematic analysis and investigation of the electromagnetic field characteristics in radial magnetic levitation bearings is conducted using the finite element simulation methodology. A mathematical model of electromagnetic force for a single magnetic pole is established to derive the relationship between electromagnetic force and parameters such as current and air gap. Finite element simulations conducted via COMSOL multiphysics yield results that are consistent with theoretical calculations, while further analyzing magnetic field distribution, air gap flux density, and electromagnetic force characteristics under saturation conditions, thereby effectively compensating for errors in theoretical computations. This study demonstrates the effectiveness of the finite element method in the design and optimization of magnetic levitation bearings, providing a more precise and reliable analytical approach for practical engineering applications.**

I. Introduction

Magnetic levitation technology is a method that uses controlled electromagnetic forces to stably suspend objects in the air, achieving contactless drive and support, thereby eliminating the friction loss and vibration caused by physical contact in traditional mechanical bearings. Since its development in the middle of the 20th century, this technology has demonstrated significant potential in various fields, including high-speed rail transportation (such as the maglev demonstration line in Shanghai), high-precision industrial equipment (such as dust-free transfer systems in the semiconductor manufacturing industry), and advanced energy systems (such as flywheel energy storage devices). Especially in today's society that pursues high efficiency, energy conservation, and high reliability, magnetic levitation technology, with its advantages of being friction-free, lubrication-free, and low-maintenance, is gradually becoming one of the key technologies for industrial transformation and upgrading [1].

Radial magnetic levitation bearings generate controllable electromagnetic forces in the radial direction of the rotor, achieving precise positioning and stable support of rotating components in the radial direction. Compared with the axial magnetic levitation systems, radial structures can more efficiently resist centrifugal forces generated by rotating loads and provide more balanced support stiffness for rotating machinery. However, the design and control of radial magnetic levitation systems face severe challenges, with the core difficulty lying in the complex spatial distribution of electromagnetic fields and the coupling characteristics of multiple physical field strengths. The precise generation of electromagnetic force depends not only on the precise control of coil current, but also on the complex effects of multiple factors such as material nonlinearity, temperature effect, mechanical deformation, and motion state. Any slight deviation in design parameters leads to decrease in suspension stability and even triggers system oscillations.

In this context, high-precision electromagnetic field simulation technology has become the core means of analyzing the working mechanism of radial magnetic levitation systems. Based on the finite element numerical simulation method, by accurately simulating the electromagnetic field distribution, eddy current effect, magnetic saturation phenomenon, and electromagnetic mechanical coupling behavior of radial magnetic levitation components under real working conditions, engineers can comprehensively predict and optimize system performance before physical manufacturing, greatly reducing the research and development costs and cycles [2]. Numerous researchers have employed various finite element simulation methods for investigating similar systems [3]. In this study, COMSOL multiphysics simulation software is used, which has many powerful functions, including multiphysics field coupling.

The core objective of this study is to systematically explore the methodology for conducting multiphysics coupling simulations of radial magnetic levitation components via COMSOL multiphysics. A complete process from model

Manuscript received: 19 September 2025; revised: 28 September 2025; accepted: 15 October 2025. *(Corresponding author: Qinglai Wei.)*

Citation: Q. Wei, M. Ren, L. Wang, L. Li, and Y. Du, Analysis of electromagnetic field of radial magnetic levitation bearings based on finite element simulation, *Int. J. Intell. Control Syst.*, 2025, 30(4), 343–348.

Qinglai Wei and Yanbin Du are with State Key Laboratory of Multimodal Artificial Intelligence Systems, Institute of Automation, Chinese Academy of Sciences, Beijing 100190, China (e-mail: qinglai.wei@ia.ac.cn; yanbin.du@ia.ac.cn).

Moxuan Ren and Long Wang are with Beijing Institute of Aerospace Control Devices, Beijing 100854, China (e-mail: renmxbit@163.com; wanglong862@njust.edu.cn).

Liang Li is with School of Mechanical Engieering & Automation, Beihang University, Beijing 100191, China (e-mail: liliang21century@126.com).

Digital Object Identifier 10.62678/IJICS202512.10238

construction, boundary condition setting, and mesh optimization to result verification is established, providing a solid theoretical foundation and technical support for the design and application of new high-performance magnetic levitation bearings [4]. The research results are expected to be directly applied to cutting-edge fields such as high-speed maglev trains and superconducting flywheel energy storage systems, promoting the practical application of magnetic levitation technology.

II. Numerical Calculation of the Operation of Magnetic Levitation with a Single Magnetic Pole

Considering the electromagnetic force application in a single direction (Y+), when two coils with opposite winding directions are energized, a magnetic circuit is formed through the iron core and air gap. The magnetic flux lines are illustrated in Fig. 1.

According to Maxwell stress formula, the relationship between electromagnetic force F generated by a single magnetic pole and the current i is given by the following equation [5]

$$F = \frac{B^2 A}{2\mu_0} = \frac{1}{2\mu_0}\left(\frac{\mu_0 N i}{g}\right)^2 A = \frac{\mu_0 N^2 A}{2g^2}\cdot i^2 \tag{1}$$

where g is the air gap thickness, N is the number of turns per coil, i is the coil current, and A is the effective magnetic flux area of the air gap.

A new coefficient is defined as $K_g = \mu_0 N^2 A/2g^2$.

$$F = K_g \cdot i^2 \tag{2}$$

The following conclusions can be drawn.

(1) The electromagnetic force is inversely proportional to the square of the air gap size $F \propto 1/g^2$.

(2) The electromagnetic force is directly proportional to the square of the current $F \propto i^2$.

When the magnetic circuit is saturated, that is, when the magnetic flux density B in the iron core (stator or rotor) reaches the saturation magnetic flux density B_s of the material, the magnetic permeability drops sharply. At this point, further increasing the current causes the magnetic flux and force to hardly increase any more, reaching the true physical saturation force.

According to the conservation of magnetic flux, the relationship formula between the saturated air-gap magnetic flux density and the magnetic flux density within the iron core can be obtained as

$$B_{g,max} = \frac{B_s S_{min}}{A} \tag{3}$$

where B_s is the core saturation magnetic flux density, and S_{min} is the minimum cross-sectional area of the core. The saturation current can be calculated as

$$i_{max} = \frac{g B_{g,max}}{\mu_0 N} = \frac{g B_s S_{min}}{\mu_0 N A} \tag{4}$$

The saturation force is approximately given by

$$F_{max} \approx \frac{B_{g,max}^2 A}{2\mu_0} = \frac{{B_s}^2 {S_{min}}^2}{2\mu_0 A} \tag{5}$$

In this design, the air gap radius is 8.65 mm, the air gap thickness g is 0.065 mm, the number of coil turns N is 130, and the thickness of the component h is 3 mm. After calculation, the effective cross-sectional area A of the air gap is 3.596×10^{-5} m^2, the minimum cross-sectional area S_{min} in the magnetic core is 2.55×10^{-6} m^2, the magnetic core material is B1T95 soft magnetic alloy, and the saturation magnetic flux density is approximately 750 mT. After calculation, K_g is 90.3828, the saturation current is 42.3 mA, the saturation electromagnetic force F_{max} is 0.1619 N, the electromagnetic force in the Y-direction is $F_{max}\cdot\cos22.5° = 0.1496$ N, and the air gap magnetic density $B_{g,max}$ at saturation is 0.1064 T.

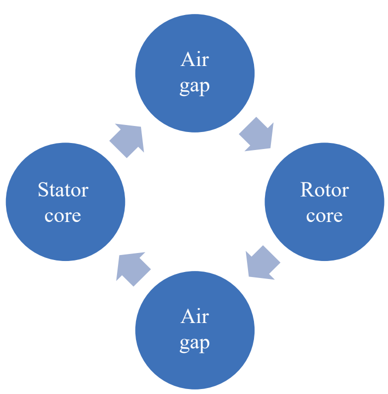

(a) Simplified schematic of the radial magnetic bearing magnetic circuit, highlighting key components and flux path

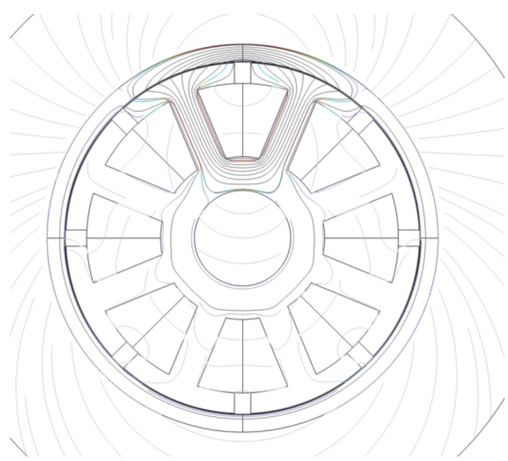

(b) Finite element model geometry of the single-pole magnetic circuit

Fig. 1 (a) Simplified schematic of the radial magnetic bearing magnetic circuit, highlighting key components and flux path. (b) Finite element model geometry of the single-pole magnetic circuit.

III. Finite Element Simulation of the Operation of a Single Magnetic Pole in Magnetic Levitation

To obtain a more accurate understanding of the magnetic field distribution of the radial magnetic levitation component and verify the above calculation results, we use the finite element simulation software COMSOL to conduct modeling and simulation of the component and analyze it.

A. Geometric Construction

In the context of academic research, given that the physical modeling of mirror magnetic levitation closely resembles a cylindrical model, a two-dimensional cross-sectional modeling approach is adopted. This method effectively reduces the time required for simulation operations.

Simultaneously, an air domain model is constructed surrounding the components. The outer boundary of this air domain is defined as an infinite source domain. This setup is designed to more accurately simulate the actual operating environment, thereby enhancing the authenticity and reliability of the simulation results in line with the requirements of academic studies.

B. Boundary Conditions

In finite element simulation, boundary conditions are the known conditions applied to the geometric boundaries of the model, representing the interaction between the analyzed system and the external environment. They are the keys to solve the mathematical equations.

(1) The magnetic core is modeled using the Ampère's law for solid conductors. Ampère's law for solid conductors is applied to the iron core to model its magnetic behavior.

(2) The air region is described using the Ampère's law for fluids. Ampère's law for solid conductors is applied to the iron core to model its magnetic behavior.

(3) A multi-turn coil condition is assigned to the winding regions, with prescribed current excitation. Multi-turn coil condition is assigned to the windings to simulate the current excitation, which is consistent with the actual driving mechanism.

(4) The force calculation feature is enabled in the rotor domain using the Maxwell stress tensor method. This method integrates the magnetic pressure over a closed surface surrounding the rotor to compute the total electromagnetic force, providing a robust and physically sound calculation.

(5) The outer boundary of the air domain is set as an infinite element domain. This boundary condition mathematically simulates an open boundary that extends to infinity, effectively absorbing outgoing magnetic fields and preventing non-physical reflections back into the simulation domain, which is essential for open-boundary field problems such as this one.

These settings ensure that the simulation closely replicates the real-world conditions.

C. Grid Division

(1) A free triangular mesh with an extremely fine size is applied to the iron core.

(2) The air gap is also meshed with a free triangular grid of extremely fine resolution.

(3) Within the coil regions, a free triangular mesh with automatic sizing is used.

(4) The remaining air subdomains are discretized using a free triangular mesh with automatic element size.

(5) The infinite element domain is constructed using a mapped mesh scheme.

D. Grid Independence Study

To ensure that the accuracy of the simulation results is not dependent on the mesh density, a grid independence study is conducted. Simulations are performed using three different mesh sizes: coarse (average element size ≈ 0.15 mm), medium (≈ 0.08 mm), and fine (≈ 0.03 mm, corresponding to the extremely fine setting used in the main study). The key output parameter, the electromagnetic force in the *Y*-direction at a current of 40 mA, is monitored for each case.

The results are summarized in Table 1. It can be observed that the difference in the calculated force between the medium and fine meshes is less than 0.5%, indicating that the solution has converged. Therefore, the extremely fine mesh setting is adopted for all subsequent simulations to achieve a high level of accuracy while maintaining computational efficiency.

Table 1 Comparison of accuracy for different grid sizes.

Mesh setting	Average element size (mm)	Electromagnetic force (N)	Deviation from fine mesh
Coarse	0.15	0.1385	~2.3%
Medium	0.08	0.1419	~0.4%
Fine	0.03	0.1425	Reference

IV. Finite Element Simulation Results and Analysis

First, we calculate the magnetic field distribution when the saturation current is applied. Set the coil current to 42.3 mA. Through the simulation calculation via COMSOL, the following magnetic flux density diagram is obtained, as shown in Fig. 2.

It can be observed that the distribution of magnetic field streamlines forms a closed loop, with the maximum magnetic flux density located at the core, reaching 0.73 T, which is close to the saturation magnetic flux density of the material (0.75 T).

The Maxwell stress distribution simulated is shown in Fig. 3, represented by the blue arrows. It can be observed that the electromagnetic force distribution is mainly concentrated in the effective area of the stator magnetic poles.

Through the numerical integration of the Maxwell stress tensor, the resultant electromagnetic force in the radial direction is calculated to be 0.1584 N, which deviates from the theoretically predicted value of 0.1619 N by 2.16%. The force in the *Y*-direction is obtained as 0.1432 N. This discrepancy can be attributed to factors such as magnetic circuit coupling

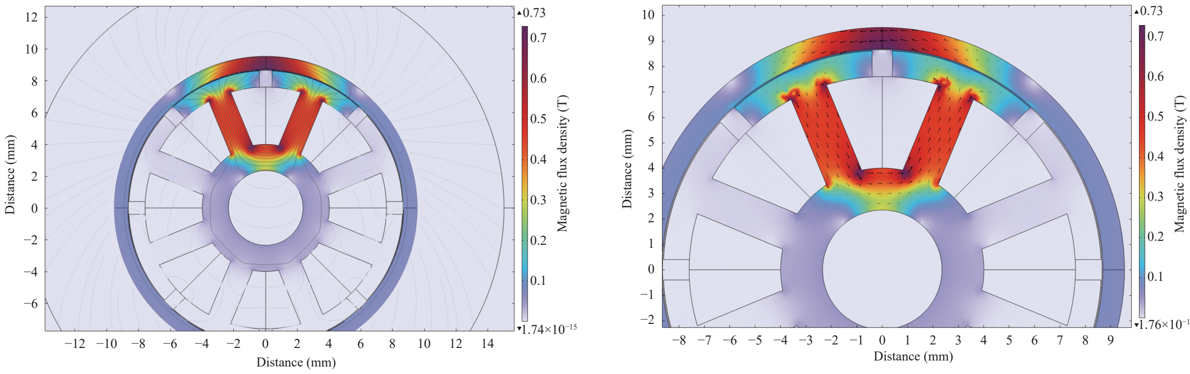

(a) Magnetic streamlines (b) Magnetic field vectors

Fig. 2 Magnetic field distribution under saturation current: (a) magnetic streamlines and (b) magnetic field vectors.

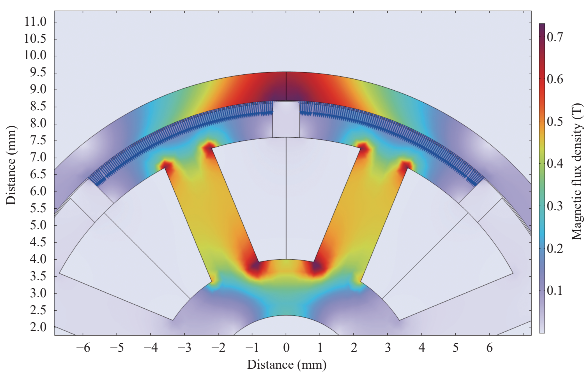

Fig. 3 Distribution of electromagnetic force under saturated current (represented by Maxwell stress).

and air gap leakage flux [5]. The sources of error are analyzed below.

(1) Core material: Theoretical calculations usually assume that the magnetic permeability of the core approaches infinity, $\mu_{\mathrm{fe}} \to \infty$ (i.e., the magnetic resistance is zero). However, COMSOL uses the actual nonlinear B-H curve. Even if the operating point has not reached full saturation, the core itself still has magnetic resistance, which will divert a portion of the magnetic flux, resulting in the air-gap magnetic flux density being slightly lower than the theoretical value. This is the main source of error.

(2) Edge effect and leakage flux: Theoretical calculations use the geometric area $A = L\theta R$. In contrast, COMSOL can precisely calculate the diffusion of magnetic flux at the edge of the air gap and the leakage magnetic flux between the poles. There are slight differences between the effective magnetic conductivity area in the simulation and the values in the theoretical formula [6].

(3) Geometric assembly and gap uniformity: Theoretical calculations assume that the air gap is absolutely uniform. In COMSOL, the meshing, whether the rotor is absolutely centered, and the geometric accuracy of the model itself all introduce errors on the order of micrometers, and the electromagnetic force is inversely proportional to the square of the air gap, which is extremely sensitive to this [7].

The air-gap flux density under saturation current is shown in Fig. 4.

It can be seen that the magnetic flux density in the air gap is not completely concentrated at the effective area of the magnetic poles, and even at the magnetic poles, it is not uniformly distributed. After calculation, the average magnetic flux density of the air gap at the magnetic poles is 0.1049 T. Compared with the calculated result of 0.1064 T, there is an error of 1.4%. Continuing to integrate the air gap magnetic flux density line, the result is 1.313×10^{-3} T·m, and integrating at the air gap at the magnetic poles gives a result of 1.258×10^{-3} T·m. The calculation shows that there is a 4.2% flux loss because of the diffusion at the edge of the air gap and the leakage magnetic flux between the poles.

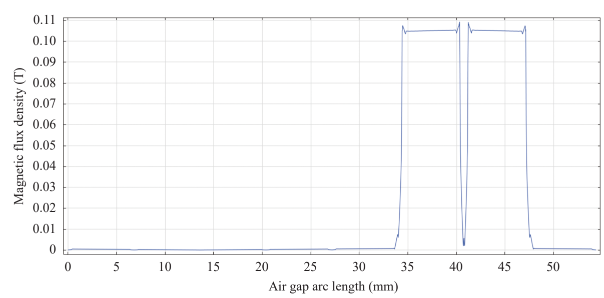

Fig. 4 Distribution of air-gap magnetic flux density under saturation current.

The distribution of Maxwell stress, as shown in Fig. 5, corresponds to the air-gap flux density distribution.

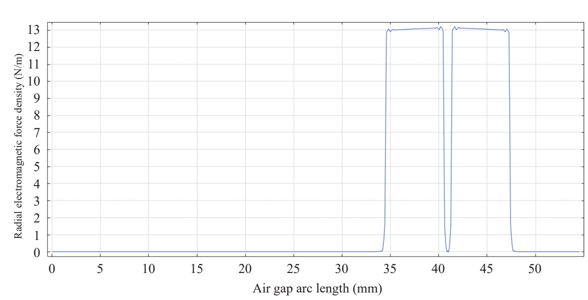

Fig. 5 Distribution of electromagnetic force (Maxwell stress) at saturation current.

Subsequently, to investigate the relationship between current and electromagnetic force, we scan the coil current I_0 within the range of 10–43 mA, with an increment of 0.5 mA. As a result, new simulation results are acquired. The relationship between the electromagnetic force and the square of the current is shown in Fig. 6.

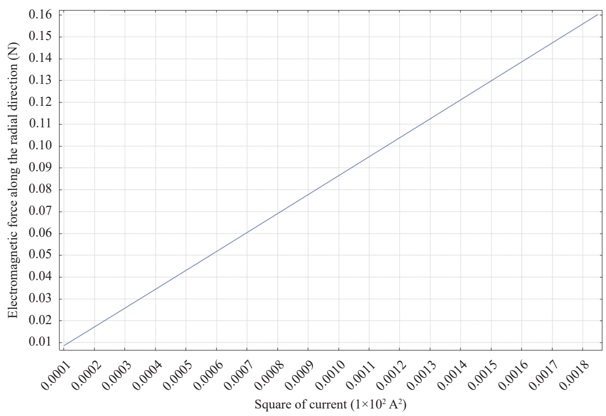

Fig. 6 Relationship between the electromagnetic force F and the square of the excitation current ${I_0}^2$. The linear relationship at lower currents validates the theoretical formula $F = K_g \cdot i^2$. The deviation from linearity beyond approximately $I_0^2 \approx 1.6 \times 10^{-3}$ A^2 (corresponding to $I_0 \approx 40$ mA) indicates the onset of magnetic saturation in the core.

In Fig. 6, the vertical axis represents the radial electromagnetic force, while the horizontal axis represents the square of the coil current I_0^2. It can be observed that there is a linear relationship between the two, consistent with the theoretical derivation of $F = K_g \cdot i^2$, where the slope of the curve defines the coefficient K_g.

Next, the result for K_g is calculated, using F/I_0^2 on the vertical axis and the current value I_0 on the horizontal axis. The resulted curve is shown in Fig. 7.

The calculated result for K_g is 90.3828, and we find that the curve approaches a maximum of approximately 86.5, which is because of some errors mentioned above. It can be observed that the overall growth rate of K_g gradually decreases. This is attributed to the fact that at low currents, the core has not yet saturated, but its magnetic permeability is finite. The core itself consumes a portion of the magnetomotive force. As the current increases, the working point of the core moves upward along the linear segment of the B-H curve, and its relative permeability μ_r gradually increases (magnetic resistance decreases), allowing more magnetomotive force to be effectively concentrated in the air gap.

V. Conclusion

The theoretical calculation conclusions are consistent with the results of the finite element simulation. COMSOL effectively validates the theoretical calculations and is capable of more closely aligning with actual computations by taking into account factors such as the B-H curve, magnetic leakage, and edge effects. This allows us to identify the sources of error we seek and the true distribution of the magnetic field. In summary, finite element simulation can validate theoretical calculations and provide supplementary insights, yielding that results are more in line with reality. Additionally, it offers a more intuitive representation of the magnetic field distribution, thereby enhancing the precision and reliability of production design.

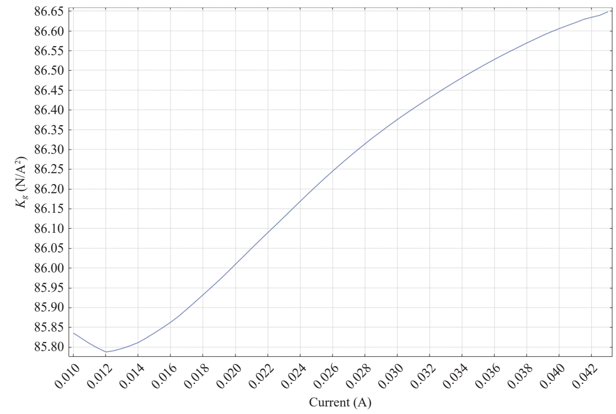

Fig. 7 Variation of the force coefficient K_g (calculated as F/I_0^2) with the coil current I_0^2. The initial increase in K_g is because of the rising relative permeability of the core material as it moves up the B-H curve, allowing more magnetomotive force to be applied across the air gap. The subsequent plateau and slight decrease near the saturation current (I_0^2 = 42.3 mA) are caused by the core entering saturation, where its permeability drops significantly.

Acknowledgment

This work was supported by the Enterprise Commissioned Project (No. E4D80223), the National Key R&D Program of China (No. 2024YFB4709100), the National Natural Science Foundation of China (No. 62425310), the Beijing Natural Science Foundation (No. L257011), and the National Defense Basic Scientific Research Program (No. JCKY2019203C029).

References

[1] W. Li, G. Zhang, X. Wang, and Q. Qiu, Integration design of high-temperature superconducting bearing and electromagnetic thrust bearing for flywheel energy storage system, *Trans. China Electrotechn. Soc.*, 2020, 35(S1), 10–18, (in Chinese).

[2] J. Sun, D. Li, Z. Li, and G. Zhang, Simulation analysis of electromagnetic performance of active magnetic suspension bearing based on finite element method, *Ind. Control Computer*, 2023, 36(3), 56–58, (in Chinese).

[3] B. Zhang, Application of finite element method in electromagnetic field of active magnetic bearing (AMB), *Electr. Switchgear*, 2004, 42(6), 30–32, (in Chinese).

[4] P. Sharma and EMPHATIC collaboration, Precise magnetic field mapping of the EMPHATIC phase 1 magnet with COMSOL, *J. Instrum.*, 2025, 20(4), P04010.

[5] W. Geng, Design of active magnetic bearing, MS dissertation, Dalian University of Technology, China, 2022, (in Chinese).

[6] G. Ding, Analysis and measurement research on electromagnetic field for magnetic bearings, MS dissertation, Wuhan University of Technology, China, 2004, (in Chinese).

[7] Y. Lou, Research on effects of multi-factor on electromagnetic force of radial magnetic bearings, MS dissertation, Wuhan University of Technology, China, 2018, (in Chinese).

Qinglai Wei received the BS degree in automation and the PhD degree in control theory and control engineering from Northeastern University, Shenyang, China, in 2002 and 2009, respectively. From 2009 to 2011, he was a postdoctoral fellow at State Key Laboratory of Management and Control for Complex Systems, Institute of Automation, Chinese Academy of Sciences, Beijing, China. He is currently a professor at Institute of Automation, Chinese Academy of Sciences, Beijing, China. He has authored four books and published over 80 international journal articles. His research interests include adaptive dynamic programming, neural networks-based control, optimal control, nonlinear systems, and their industrial applications. He was a recipient of the IEEE/CAA Journal of Automatica Sinica Best Paper Award, the IEEE System, Man, and Cybernetics Society Andrew P. Sage Best Transactions Paper Award, the IEEE Transactions on Neural Networks and Learning Systems Outstanding Paper Award, the Outstanding Paper Award of Acta Automatica Sinica, and the Zhang Siying Outstanding Paper Award of the Chinese Control and Decision Conference. He was also a recipient of the Shuang-Chuang Talents in Jiangsu Province, China, and the Young Researcher Award of Asia-Pacific Neural Network Society. He has been the vice president of the IEEE Computational Intelligence Society Beijing Chapter since 2022. He was the general co-chair of the 2019 Symposium of Parallel Intelligence, the invited session chair of the IEEE 8th Data Driven Control and Learning Systems Conference, the special sessions chair of the 25th International Conference on Neural Information Processing, the program co-chair of the 24th International Conference on Neural Information Processing, and the registration chair of the 12th World Congress on Intelligent Control and Automation (WCICA2016) and the 2014 IEEE World Congress on Computational Intelligence (WCCI2014). He is a guest editor for several international journals. He is an associate editor-in-chief/the deputy editor-in-chief of the *IEEE/CAA Journal of Automatica Sinica*, *Neurocomputing*, and *Acta Automatica Sinica*.

Moxuan Ren received the BSc and MSc degrees from Beijing Institute of Technology, Beijing, China, in 2017 and 2022, respectively. She is currently an engineer at Beijing Institute of Aerospace Control Devices, Beijing, China. Her research interests include electrical systems of inertial sensors and image algorithms for navigation devices.

Long Wang received the BSc and MSc degrees from Beijing Institute of Technology, Beijing, China, in 2012 and 2014, respectieely. He is currently pursuing the PhD degree at Nanjing University of Science and Technology, Nanjing, China, and a senior engineer at Beijing Institute of Aerospace Control Devices, Beijing, China. His research interest includes inertial instrument design.

Liang Li received the BSc and MSc degrees from Northwestern Polytechnical University, China, in 2003 and 2007, respectively. He is currently pursuing the PhD degree at Beihang University, Beijing, China. His research interest includes inertial instrument design.

Yanbin Du received the BS degree from Jilin University, Changchun, China, in 2011, and the MS degree in aero-engine control and the PhD degree in control theory and control engineering from Nanjing University of Aeronautics and Astronautics, Nanjing, China, in 2017 and 2023, respectively. He is currently an assistant researcher at Institute of Automation, Chinese Academy of Sciences and the State Key Laboratory of Multimodal Artificial Intelligence Systems, Beijing, China. His research interests include reinforcement learning, fault-tolerant control and applications in autonomous decision-making, and fault-tolerant cooperative control for unmanned aerial vehicles.